

RSC Advances



This is an *Accepted Manuscript*, which has been through the Royal Society of Chemistry peer review process and has been accepted for publication.

Accepted Manuscripts are published online shortly after acceptance, before technical editing, formatting and proof reading. Using this free service, authors can make their results available to the community, in citable form, before we publish the edited article. This *Accepted Manuscript* will be replaced by the edited, formatted and paginated article as soon as this is available.

You can find more information about *Accepted Manuscripts* in the [Information for Authors](#).

Please note that technical editing may introduce minor changes to the text and/or graphics, which may alter content. The journal's standard [Terms & Conditions](#) and the [Ethical guidelines](#) still apply. In no event shall the Royal Society of Chemistry be held responsible for any errors or omissions in this *Accepted Manuscript* or any consequences arising from the use of any information it contains.

ARTICLE

Novel CuO/Chitosan nanocomposite thin film: Facile hand picking recoverable, efficient and reusable heterogeneous photocatalyst

Cite this: DOI: 10.1039/x0xx00000x

Received 00th January 2012,
Accepted 00th January 2012

DOI: 10.1039/x0xx00000x

www.rsc.org/

P. Senthil Kumar¹, M. Selvakumar², Sundaram Ganesh Babu³, Saravana Kumar Jaganathan⁴, S. Karuthapandian^{1*}, Santanu Chattopadhyay²

The present work demonstrates a new simple hand picking technique for the 100% recovery of photocatalyst. CuO nanospheres was synthesized by simple wet chemical method and subsequently embedded into the biopolymer matrix (chitosan) under mild condition by solution casting method and reported its photocatalytic application towards the degradation of organic pollutants for the first time. The crystal structure, optical properties, surface and bulk morphology were discussed in detail. ICP-OES analysis shows 3.025 % copper was embedded on the CS matrix. Efficiency of the CuO/chitosan was evaluated against the degradation of Rhodamine B dye as a probe. The combination of CuO nanospheres with chitosan leads to the higher efficiency of up to 99% degradation of the dye with 60 minutes of irradiation. This may be attributed by many features such as the slow electron hole pair recombination rate of nanosized CuO in the biopolymer matrix, large surface area of CuO and high absorption efficiency of the chitosan. The major advantage of this present protocol is that it is not only restricted to azo type dyes but also adopted for different kind of organic pollutants. For all the type of organic contaminants tested, the CuO/CS NCF photocatalyst showed excellent activity. This facile hand picking recovery and recyclability of this novel thin film likely opens up a new straightforward strategy in effective photocatalytic degradation of organic contaminants process.

Keywords: CuO/chitosan, composite film, hand picking recovery, photo degradation, reusable

Introduction

Photocatalysis is a “green” technique which offers a great potential in environmental remediation such as the photodegradation of the organic pollutants in the wastewater from the industrial drain. In this regard, some metal oxides nanoparticles were reported with good photocatalytic performances¹⁻³. However, in the case of support free heterogeneous metal oxide nanocatalysts, the separation⁴ and recycling of the utilized nanoparticles are very tedious tasks at present⁵, especially in large scale treatment processes. Moreover, turbidity of the high concentrated catalyst suspensions is responsible of a light shadowing effect, which can drastically lower the photocatalytic activity. Therefore, development of high performance photocatalyst with an easily recycling property is highly desired for such applications^{6, 7}. In this regard, impregnation of the photocatalysts over a proper solid matrix might be an efficient strategy to recover the photocatalyst for effective recycling.

Embedding of inorganic nanomaterial (photocatalyst) into a polymer matrix offers a number of potential advantages and presenting significant value in environmental applications, including facile incorporation within continuous reactors and eases of recovery

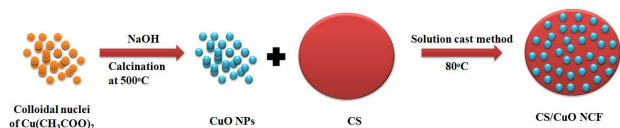
and reuse, especially in large scale⁸. Owing to its multifunctional behaviour such as easy processing, compatibility etc., polymers are currently being widely used as an excellent solid support for the metal nanocomposites. Recently, a number of studies^{8, 9} have focused on the use of natural organic polymers as a supporting material for photocatalytic compounds, and more especially in the preparation of heterogeneous catalysts¹⁰⁻¹³.

In recent years particularly chitosan (CS) biopolymer has exhibited multifunctional performance with TiO₂, ZnO, and CdS in heterogeneous photocatalysis technology which gives a high percentage photo degradation of environmental pollutants. In addition, immobilized nanosized photocatalysts on the chitosan bio-matrix can effectively prevent the agglomeration of nanoparticles during growth and also overcome the difficulty in recovery of nanosized powder materials from the reaction medium^{14, 15}. Although in the solid matrices supported photocatalytic systems, recovery of the catalyst is carry forward either through filtration or by centrifugation which in turn causes lose of photocatalyst to an extent. Hence, in the present study, an attempt has been made to develop a facile hand picking technique for the biopolymer supported (CuO/CS) nanocomposite thin film (NCF) as a

photocatalyst which was prepared by solution cast method for the first time to enhance photocatalytic performance. Typical Rhodamine B (RhB) was selected as a model hazardous dye to evaluate the feasibility of the adsorption – photocatalytic degradation by nano CuO/CS NCF under visible light irradiation. The high performance of CuO/CS NCF was expected to result in complementation of advantages of each component and hence provide economically feasible and environmentally friendly method in the treatment of effective dye degradation. 100 % recovery of the photocatalyst was demonstrated and reasonable reusability was observed.

Results and discussion

The formation mechanism of CuO/CS NCF prepared by solution cast method is given in scheme 1



Scheme 1: Schematic Representation of synthesis of Novel CuO/CS NCF

When copper acetate was added to the millipore water, a blue color transparent aqueous solution was obtained. Further, the CuO nanospheres were obtained by precipitation of aqueous copper acetate with sodium hydroxide followed by calcination. Finally the CuO was embedded in the CS matrix by solution cast method.

Characterization of CuO/CS NCF

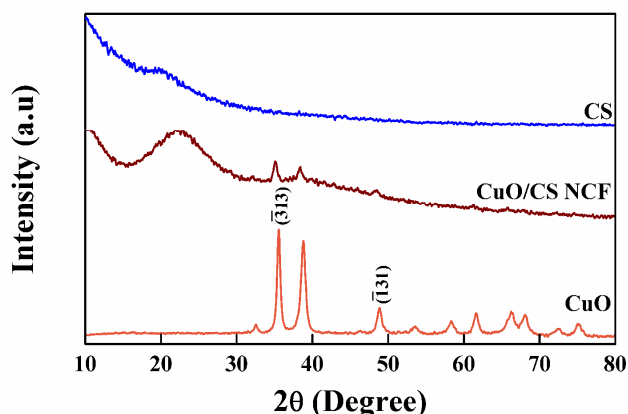


Figure 1: XRD patterns of CS, CuO/CS NCF and CuO

Figure 1 shows the WXR of the pristine nano CuO, CS and CuO/CS NCF. For pure CuO nanocrystal, the typical monoclinic diffraction patterns was found, which can be indexed as per the standard data (JCPDS No. 01-1117). The diffraction peaks at 2θ regions of 35.5 and 38.7° was related to the monoclinic structure with $(\bar{3}13)$ and $(\bar{1}31)$ orientation, respectively. The same characteristic peaks are observed in the CuO/CS nanocomposites film with less intensity, it confirmed the formation of CuO/CS nanocomposites. The peak at 20.2° is a characteristic diffraction peak for the CS; the peak was broad due to the amorphous nature of the polymer. Addition of CuO to the CS matrix leads to increase the crystalline nature of the composite films and the peak is shifted

towards higher 2θ value. In addition, the crystallite size was calculated from Scherer's equation¹⁶ using the reflections of plane $(\bar{3}13)$ and the value is 85.2 nm and 45.5 nm for pristine CuO and CuO/CS NCF respectively. The reduction in crystallite size of CuO by the formation of CuO/CS NCF indicates the better interaction between the CS and CuO.

Figure 2 shows the FESEM photomicrographs of the pristine CS film and CuO/CS NCF. The surface of the CS film was pretty smooth as can be seen from Figure 2 (a). However, by the introduction of CuO nanospheres into the CS matrix (Figure 2 b), some well dispersed and fine granules were also been observed which confirmed the formation of NCF of CuO/CS. CS matrix could prevent the agglomeration of the CuO nanospheres and provide larger surface area for the photocatalytic reaction *via* adsorption process.

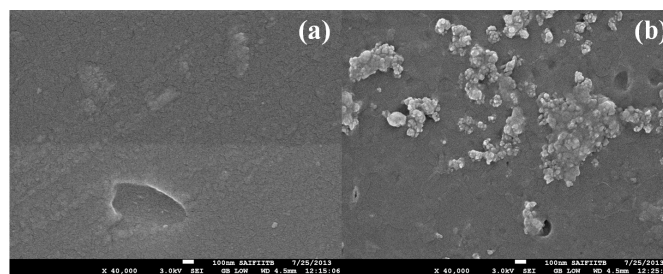


Figure 2: FE-SEM micrographs of as synthesized (a) pure CS and (b) CuO/CS NCF

The TEM images (Figure 3) revealed that there existed many pleats on the surface of the CS.

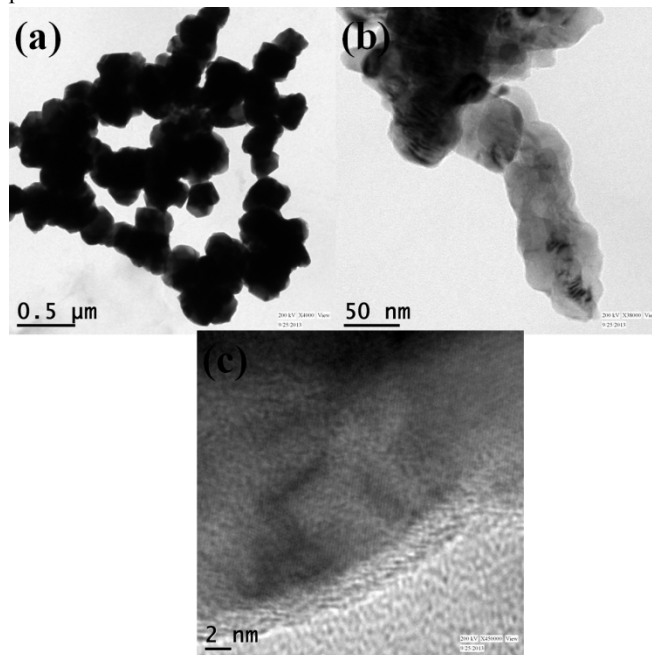


Figure 3: (a) TEM images of as synthesized CuO, (b) High magnification TEM images of as synthesized CuO/CS NCF (c) Lattice fringes of as synthesized CuO/CS NCF

The size of the CuO nanospheres embedded into the CS matrix is ~ 50 nm as it can be seen from the TEM micrograph (Figure 3 b and 3 c) and the clear crystals were also observed. It unveils the clear

lattice fringes, thereby indicating that the nano CuO were structurally uniform and contain no defects such as dislocations or stacking faults after embedded into CS matrix. The lattice spacing of 0.244 nm almost agrees with the (313) plane of cubic-structured CuO (the lattice spacing is 0.247 nm for (313) according to JCPDS file no. 01-1117).

Furthermore, presence of CuO in CS matrix was confirmed by EDX analysis and it shown in Figure 4. In addition, ICP analysis was also carried out to find out the percentage of metal present in the CS matrix. It was confirmed that 3.025 % copper were embedded on the CS matrix. It is well matched with our EDX spectrum and experimental procedure.

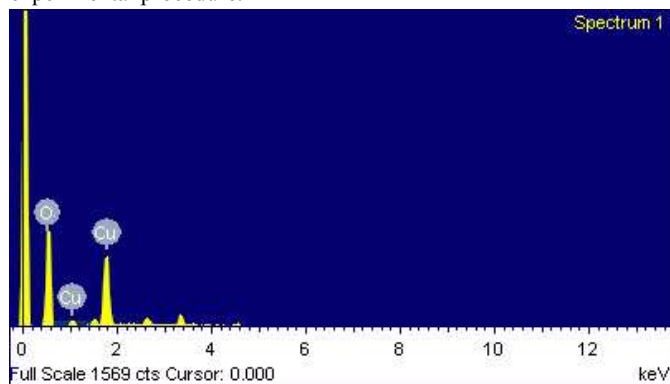


Figure 4: EDX spectrum of as synthesized CuO/CS NCF

The optical absorption properties and the migration of light induced electrons and holes of semiconductor¹⁷, which depends upon the materials electronic structure, are known as key factors in determining the photocatalytic activity¹⁸. As shown in figure 5 (a), there is significant absorption edge at around 560 nm revealing that the photocatalytic activity in the visible range.

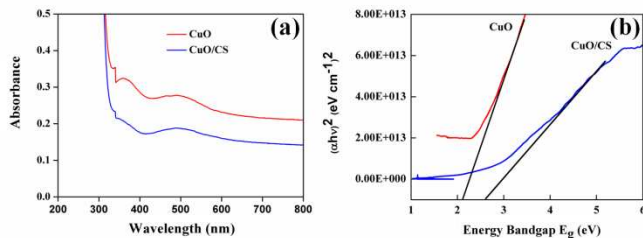


Figure 5: (a) DRS UV-Visible absorption spectrum of CuO and CuO/CS NCF, (b) Energy gap (Tauc plot) of CuO/CS NCF

Moreover, the tauc plot (figure 5 b) is plotted to estimate the band gap of the prepared pristine CuO and CuO/CS NCF, and the band gap value is 2.1 and 2.60 eV respectively. In general, CuO has the band gap value of around 1.4 eV but interestingly the band gap value is amplified when it is wrapped up in the CS matrix.

In order to understand more on the effect of porosity and generated macro porous of CuO/CS NCF on its optical and photoelectric properties, the photoluminescence spectroscopy analysis was performed. Figure 6 shows the room temperature PL emission spectra of pure CuO, bare CS and CuO/CS NCF. CS shows a broad emission peak at 510 nm.

It can be seen that there are three different emission bands in the PL spectrum of pure CuO. The peaks centered at 495, 555 and 600 nm were corresponding to the blue and green emission bands. The blue emission might be originated from the electron excitations and green emission was due to the deep level defects. But in the case of CuO/CS NCF, the emission intensities were almost negligible which might be due to the fact that the prevention of electron-hole pair recombination in CuO by CS. Because of this restricted recombination, the holes and electrons were freely available for the generation of $\cdot\text{OH}$ and $\cdot\text{OOH}$ radicals which are responsible for the enhanced photocatalytic degradation.

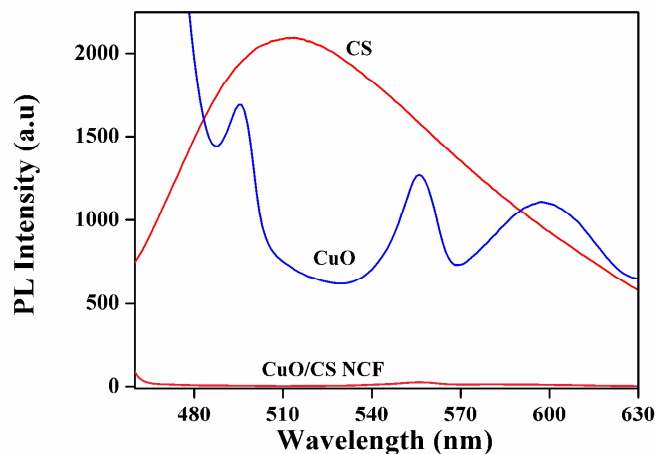


Figure 6: Photoluminescence spectrum of pure CS, pure CuO and CuO/CS NCF

The chemical composition of the synthesized CS, CuO and CuO/CS NCF was examined by FTIR-ATR spectroscopy and it is shown in Figure 7. For the pristine CuO, the peak at 484 cm^{-1} and 424 cm^{-1} are the characteristic peak of CuO. The stretching and bending vibration of CS at 3437 cm^{-1} and 2925 cm^{-1} were attributed to the amino ($-\text{NH}_2$), hydroxyl ($-\text{OH}$) groups, and $-\text{CH}_2-$, $-\text{CH}_3$ aliphatic groups, respectively.

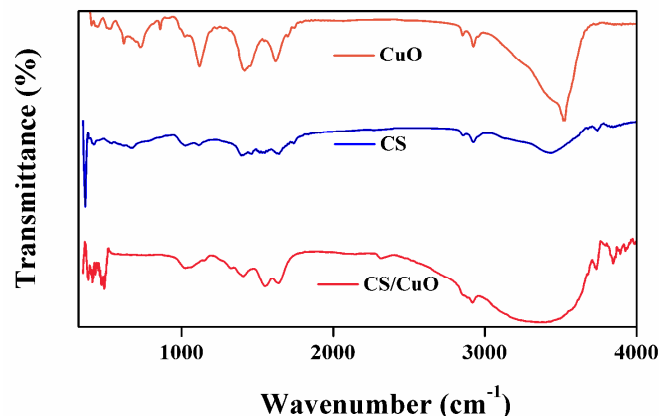


Figure 7: FT-IR ATR Spectrum of as synthesized CuO, CS, and CuO/CS NCF

Strong absorption band at 1643 cm^{-1} and 1548 cm^{-1} were attributed to the bending vibration of $-\text{NH}_2$ group and bending vibration of $-\text{OH}$ group, respectively. In the spectrum of CuO/CS NCF, the 3437 cm^{-1} peak of N-H and O-H stretching vibration of CS

was shifted to 3370 cm^{-1} and became wider, the peak at 1643 cm^{-1} due to N-H bending vibration was shifted to 1637 cm^{-1} and the 1548 cm^{-1} peak of O-H bending vibration was shifted to 1550 cm^{-1} . Moreover, the shift from 484 cm^{-1} to 469 cm^{-1} and 424 cm^{-1} to 419 cm^{-1} the characteristic peak of CuO resulted from the strong interaction between CS and CuO. This result indicates that the CS and CuO are well linked together.

Thermal stability of the pure CS, CuO and CuO/CS NCF was investigated by TG-DTA and shown in Figure 8.

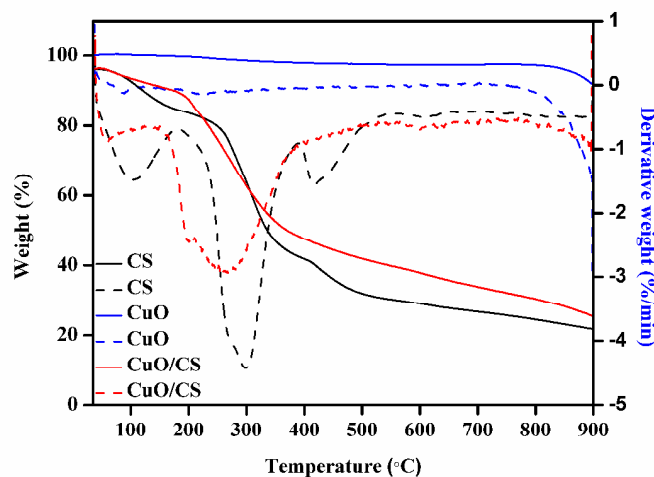


Figure 8: TG-DTA spectrum of pure CS, CuO and CuO/CS NCF

For pure chitosan the weight loss occurred at three stages. The first one was started at $55\text{ }^{\circ}\text{C}$ and ended at $157\text{ }^{\circ}\text{C}$ with a weight loss nearly about 10 % which may be due to the loss of water in chitosan films. The second stage was started at $243\text{ }^{\circ}\text{C}$ and ended at $352\text{ }^{\circ}\text{C}$ with a weight loss of 52 % which was assigned to the decomposition of chitosan films. The third stage was started at $392\text{ }^{\circ}\text{C}$ and ended at $477\text{ }^{\circ}\text{C}$ which may be attributed to the vaporization and elimination of volatile products¹⁹. The inorganic material, metal oxides generally do not decompose in thermal condition up to their melting point. The TGA curve of CuO has no significant weight loss. That clearly indicates that the CuO exists in its pure form. CuO/CS NCF has two distinct weight losses. The first stage with 3 % weight loss were started at $46\text{ }^{\circ}\text{C}$ and ended at $109\text{ }^{\circ}\text{C}$ which may be attributed to the removal of water from the CuO/CS NCF. The sudden weight loss of 51 % ($182\text{ }^{\circ}\text{C} - 365\text{ }^{\circ}\text{C}$) was the degradation of the polymer²⁰. In addition, the residual weight percentage at $700\text{ }^{\circ}\text{C}$ was proportional to the inorganic content and it is owing to CuO. The residual weight of the CuO/CS NCF was 10 % more than that of pure chitosan film. The TG-DTA results shows the CuO nanoparticles may immobilized onto the CS matrix.

Liquid-phase adsorption of RhB by CuO/CS NCF

Liquid phase adsorption studies were carried for the CS, CuO and CuO/CS NCF to find out the adsorption efficiency of the catalyst and result is shown in Figure 9. Among three, both CS and CuO/CS NCF showed almost equal adsorption efficiency. Indeed, the

photocatalytic efficiency of CuO/CS NCF was superior which is owing to the high adsorption behaviour.

Photocatalytic degradation of RhB solution under visible light irradiation

The potential efficiency of the CuO/CS NCF was evaluated by the photocatalytic activity towards the degradation of RhB dye. RhB is relatively stable in aqueous solution upon visible light irradiation. Furthermore, the photocatalytic studies confirmed that catalyst and light source both are necessary for the photocatalysis reaction to occur. Therefore, the RhB dye degradation is caused by the photocatalytic reaction of CuO/CS NCF. The characteristic absorption peak of RhB at around 553 nm was used to monitor the photocatalytic degradation process. Figure 10 (a) shows the UV-Vis absorption spectra of the aqueous solution of RhB with CuO/CS NCF as catalyst for various durations.

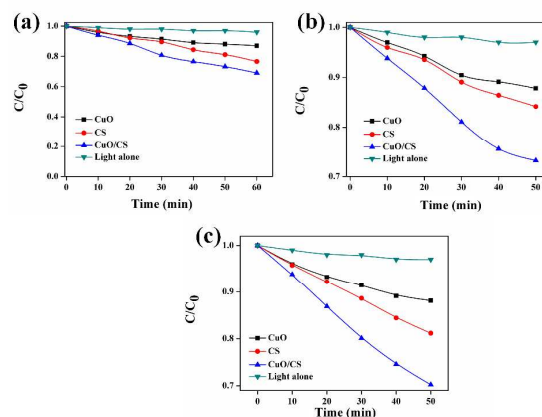


Figure 9: Liquid phase adsorption by CuO, CS and CuO/CS (a) RhB (b) CV and (c) CR

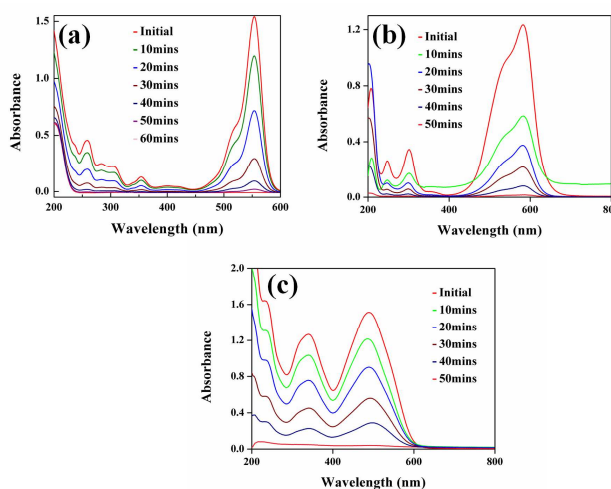


Figure 10: Absorption spectra of a solution of RhB under visible light illumination with CuO/CS NCF (a) RhB (b) CV and (c) CR

The color of the dispersed solution was disappeared after 60 min. Hence the CuO/CS NCF photocatalyst degrade $\sim 99\%$ of RhB at 60 min under visible light illumination which clearly pointed out the efficacy of the catalyst.

In addition to the azo dye, (Crystal Violet) CV was also chosen to evaluate the photocatalytic activity of the CuO/CS NCF. As like RhB, the CV solution was also showed no decolorization in present of catalyst alone under dark or without catalyst under light source. UV-vis spectral changes significantly during the photocatalytic degradation of CV in the CuO/CS NCF and it were shown in figure 10 (b). On irradiation with UV light the absorption peak at 582 nm of CV solution decreases gradually and the solution (10 μM) becomes colorless after 50 minutes irradiation.

The photocatalytic degradation study was also carried out for (Congo Red) CR. UV-vis spectral changes notably during the photocatalytic degradation of CR in the CuO/CS NCF and it were shown in figure 10 (c). During the UV light irradiation, the characteristic absorption bands of the dye (488 nm and 339 nm) decrease gradually and the solution (10 μM) was almost colorless after 50 minutes irradiation. All these results implies that the CuO/CS NCF photocatalyst can be used as an efficient degradation catalyst for different kind of dyes including azo type which is an added advantage of the present catalyst.

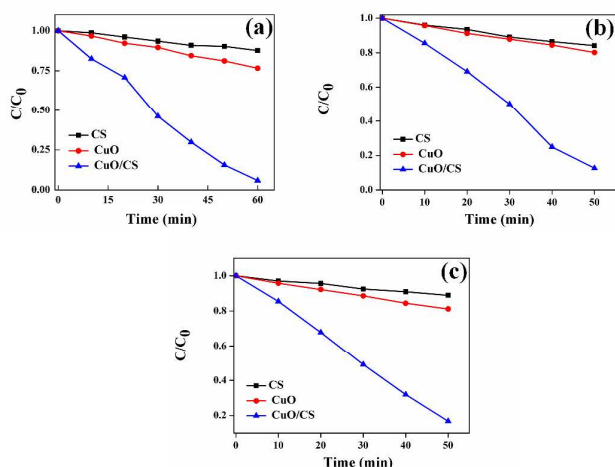


Figure 11: Photodegradation with CuO, CS and CuO/CS (a) RhB (b) CV and (c) CR

Moreover, comparisons of photocatalytic activity among the pure CS film, pure CuO and CuO/CS NCF are shown in figure 11. Among all, the CuO/CS NCF shows the highest photocatalytic degradation rate of all dyes used. The degradation efficiency of the pristine CS and pure CuO were much lower than those of the CuO/CS NCF and the corresponding C/C_0 values. Lowering of C/C_0 value for pristine CS films may be attributed to its high adsorption ability towards dye molecule. Therefore, the photocatalysis and adsorption had remarkable synergistic effect on the dye degradation.

It is well known that the heterogeneous photocatalysis mainly occur in molecule interfacial layers, so the adsorption properties between the reactants and photocatalyst surface play an important role in determining overall reaction rate. It should be considered that the modification of the CS surface by embedding the CuO would provide an effective environment for increasing the surface active sites for the dye-semiconductor interaction, which may also increase the photo degradation processes. In addition, CS itself adsorbs dye molecules, which were continuously supplied to CuO for degradation, and thus contributes to increase the efficiency of CuO significantly. According to the observation from electron

microscopy, the surface of CuO/CS NCF was rough and porous, which could increase the surface area of the composite to improve its adsorption ability²¹.

In order to minimize the waste of chemicals it is necessary to make sure the optimized amount of photocatalyst required for the effective and greener way degradation of these environmentally hazardous dyes. And also it is paramount important to evaluate the maximum efficiency of CuO/CS NCF photocatalyst by increasing the concentration of dyes.

The amount of CuO/CS NCF photocatalyst needed for the effective degradation of dyes was investigated by using different dosages of CuO/CS NCF varying from 25 mg to 75 mg as shown in figure 12. It is so obvious that the rate of photodegradation of dyes increased with increasing photocatalyst amount. This observation may be caused by the increase in the number of photons adsorbed on the photocatalyst or the number of activated molecules adsorbed on the photocatalyst surface with increase in amount of photocatalyst.

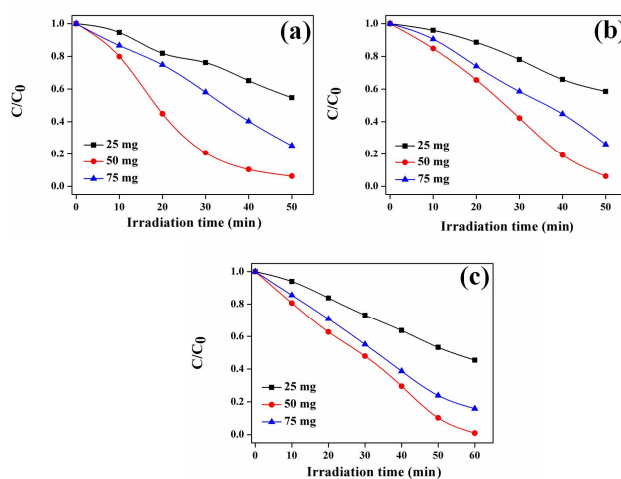


Figure 12: Photodegradation by CuO/CS at different amount of catalyst loading (a) RhB (b) CV and (c) CR

Initially, the increase of photocatalyst quantity increased the degradation percentage and an utmost efficiency was observed with 50 mg of photocatalyst. But further increase of catalyst loading showed a similar activity as like in other catalytic systems, i.e. after certain amount of catalyst the photocatalytic activity remain in same rate. This is due to the fact that excess loading of catalyst prevent the light penetration into the surfaces so that the reaction proceeded at similar rate after reaching the optimum amount. Hence 50 mg of photocatalyst was noted as an optimum catalyst dosage and used for further photoreactions.

Similarly, it is necessary to know that the effectiveness of the photocatalyst against the high concentrated dye solution. Therefore the photodegradation of dyes was studied by varying the concentration from 1 μM – 25 μM . The degradation of the dye over a concentration range from 1 μM – 25 μM is shown in Figure 13. It was worthy noted that as the dye concentration increases from 1 μM – 15 μM , the C/C_0 after continuous illumination reduces around 99% for all three dyes.

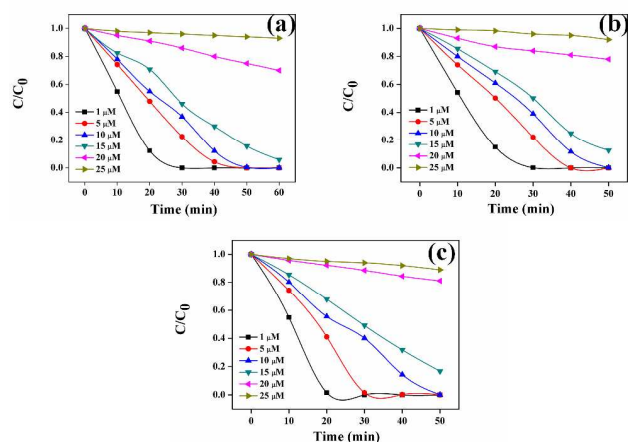


Figure 13: Photodegradation by CuO/CS at different concentrations of (a) RhB (b) CV and (c) CR

At a fixed light intensity, the decrease in degradation of dyes with an increase in dye concentration can be attributed to the greater amount of dye competing for the degradation and the reduction in the light intensity that reaches the CuO/CS NCF surface. At very high concentrations, most of the light is screened by the solution and fewer photons are able to reach the CuO/CS NCF surface. Thus, the generation of electron-hole pairs is greatly reduced and in turn the dye degradation is reduced due to absence of oxidizing species.

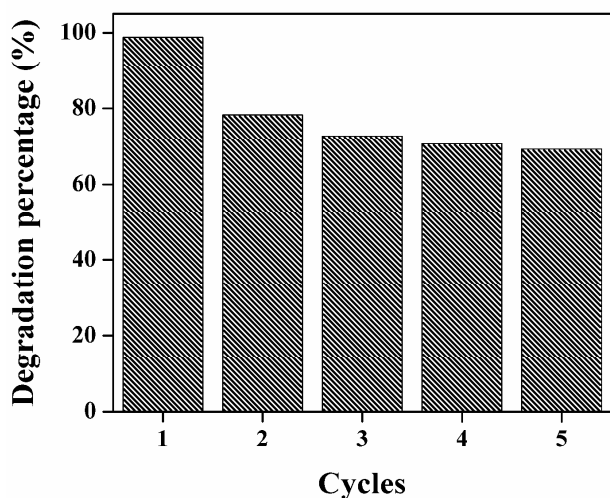


Figure 14: Reusability efficiency of CuO/CS NCF

To examine the stability of photocatalysts, recycling experiments were carried out and the results are presented in figure 14. For each cycles, the photocatalysts were reused for the degradation of fresh RhB solution under visible light irradiation. The decolorize percentage of RhB solution for 5 times use were 98.8, 78.3, 72.8, 70.6 and 69.2 % after 60 minutes of irradiation, respectively. The results show that the catalytic activity of the CuO/CS NCF was decreased in the second run and subsequently maintained relative stability. The decrease of degradation percentage may be due to the adsorption of intermediate products on the photocatalyst active sites, which rendered them unavailable for degradation of fresh dye solution¹³. However, 69.2 % of RhB was decolorized successfully for the 5th use of the photocatalysts, which indicated that the CuO/CS NCF catalyst could be reused.

The stability of the CuO/CS before and after the photocatalytic reaction was evaluated using XRD which is shown in Figure 15.

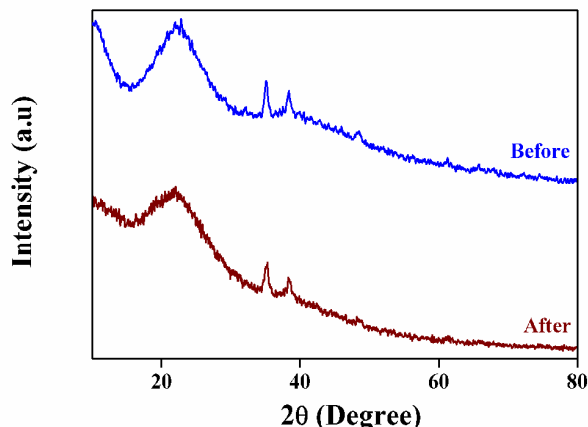


Figure 15: Comparison of XRD patterns of CuO/CS NCF before and after the photocatalytic reaction.

The XRD pattern CuO/CS NCF after the photocatalytic reaction was evidently suggests that the intensity of the characteristic peaks of CuO was decreased. The decrease in the intensity was might be due to the photocorrosion and photo dissolution of the catalysts. These results suggested that the catalyst was relatively stable one.

The rate of degradation of dyes in the presence of benzoic acid was investigated and shown in figure 16. The results indicated that the addition of benzoic acid into the reaction medium suppresses the photo degradation since it scavenges the active \bullet OH radical and slow down the photo degradation process. When the concentration of the benzoic acid was increased, the photo degradation percentage was decreased further. This is because of the reduced amount of \bullet OH radical produced from the electron-hole pairs of the photocatalyst which leads to the decrease in photo degradation of the dyes.

To support the involvement of \bullet OH radical in the photo degradation, the reaction were carried out by some more substances like azide ion, acrylamide, Triphenyl phosphine (TPP) and Rose Bengal (RB) (Figure 17). It was found that acrylamide enhances the photodegradation in the presence of catalysts indicates the absence of involvement of superoxide mechanism. Azide ion and Rose Bengal is singlet oxygen generator, it generally supports the superoxide radical mechanism²². It creates singlet oxygen which may absorb the electron from the conduction band and produces the superoxide radical ion.

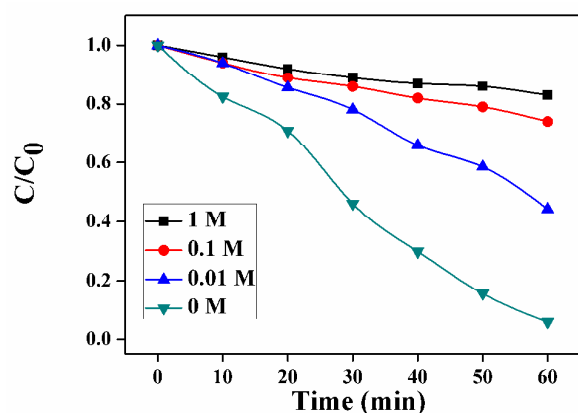


Figure 16: Photodegradation by CuO/CS in the presence of different concentrations of benzoic acid

Furthermore it precedes the photocatalytic mechanism in the conduction band by up taking the superoxide radical ion. Azide ion, a singlet oxygen quencher, fails to suppress the photodegradation indicating the absence of involvement of singlet oxygen in the surface photocatalysis. RB, a singlet oxygen generator decreases the photodegradation indicates that the superoxide anion does not involve in the degradation reaction. Sacrificial electron donor TPP generally enhances the photocatalytic reactions which involves superoxide radical ion²³. In the present system it fails to enhances the photodegradation rate which clearly indicates that the reaction lead only by the formation of $\cdot\text{OH}$ radical and not by the superoxide radical anion.

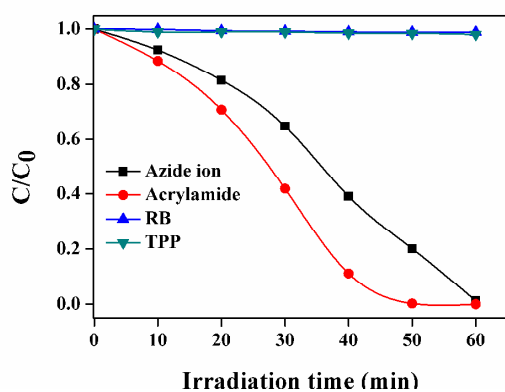
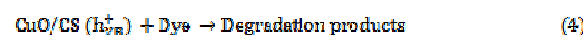
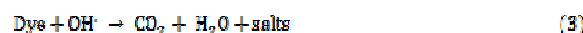
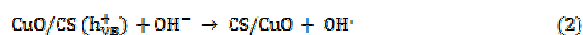
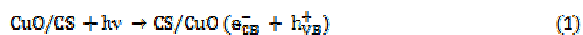


Figure 17: Photodegradation by CuO/CS in the presence of different substrates.

When the catalyst is irradiated with visible light, electrons (e^-) in the valance band (VB) are excited to the conduction band (CB) with simultaneous generation of the same number of holes in the VB (equation 1). Similarly, the photo induced holes can be easily trapped by OH^- to produce hydroxyl radical species ($\text{OH}\cdot$) (equation

2), which is an extremely strong oxidant for the partial or complete mineralization of organic pollutants (equation 3 & 4)¹⁴.

The active electrons (e^-) and holes (h^+) are generated when the incident photon energy is greater than the band gap. The narrow band gap of CuO tends the electrons (e^-) and holes (h^+) pairs to recombine quickly [Figure 18].

However, when nano CuO particle was embedded into CS, more photo-generated electrons could be captured by adsorbed O_2 on the surface of CuO/CS NCF, which may restrain the recombination between photo-generated electrons and holes to improve the photocatalytic activity of CuO/CS NCF²⁴.

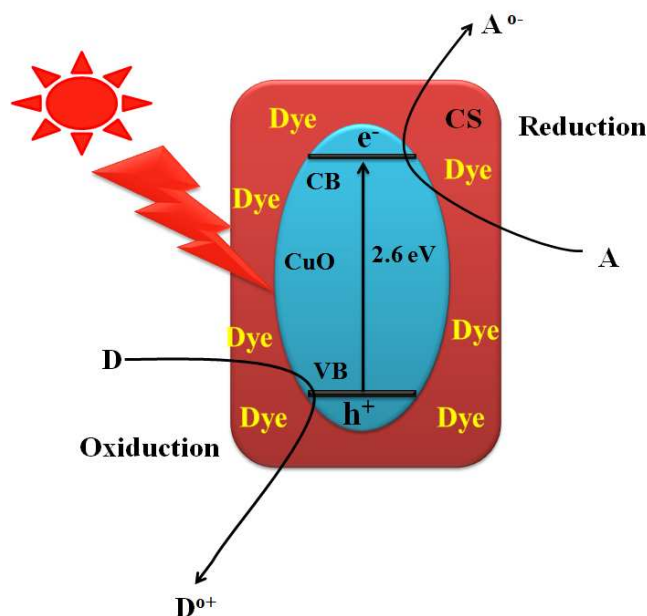


Figure 17: Mechanism of the photodegradation of RhB

Experimental Section

Materials

All chemicals and solvents used were of analytical grade from Merck. Commercial grade RhB, CV and (CR) were used. Throughout the experimental work, Millipore water was used.

Synthesis of nano CuO

CuO was synthesized by simple wet chemical method. 20 mL of 0.1 M copper acetate solution in deionized water was taken and pH of the solution was adjusted to 6 by adding dilute acetic acid. Then the reaction mixture was mixed with 20 mL of 0.5 M NaOH solution to obtain brownish precipitate. Then it was washed with water and ethanol for several times. After washing, the precipitate was dried at 120 °C for 12 h and then it was subjected to calcination at 500 °C for 4 h.

CuO/ CS NCF Preparation

In a typical experiment, 0.5 g of CS was dissolved in 20 mL of 1 % acetic acid and it was stirred vigorously to attain the homogeneous gelatinous form. Then the desired amount of nano CuO was initially dispersed into the CS matrix by sonication. The reaction mixture was stirred vigorously until it became a homogeneous mixture. To the above reaction mixture, 0.2 M NaOH was added in order to neutralize the solution. Then the homogeneous mixture was poured into a petri dish and dried at room temperature. Further the films

were dried in an oven at 60 °C and subsequently dried films were peeled off from the petri dish.

Characterization

Surface morphology of the nanocomposites films were studied by FESEM with an (Model SUPRA 40 Field Emission Scanning Electron Microscope) acceleration voltage at 30 kV. The bulk morphology, dispersion and distribution of nano CuO in the CS matrix were observed through transmission electron microscopy (TEM) using a JEM 2100. Wide angle X-ray diffraction (WXR) was performed to examine the crystal structure of the nano CuO and its nanocomposites using a Philips PW-1710 X-ray diffractometer (Eindhoven, The Netherlands). ICP-OES was performed to found out the percentage of copper in the composite using Optima 5300 DV ICP-OES. Shimadzu UV Vis-1800 spectrometer was used to analyze the samples.

Liquid-phase adsorption of RhB by CuO/CS NCF

Since the photo-oxidation reaction usually takes place on the photocatalysts surface, the adsorption of pollutant on photocatalysts are important for the photocatalytic process. 50 mg of CuO/CS NCF was added to 100 mL of RhB solution (10 µM of initial concentration). The adsorption system was continuously stirred in dark. The supernatant was withdrawn periodically and analyzed using maximum absorption wavelength (λ_{\max}) of 553 nm with the help of UV-Visible spectrometer.

Photocatalytic degradation of RhB solution under visible light irradiation

The photocatalytic activity of CuO/CS NCF was evaluated by employing a immersion type photo reactor (Heber, India) in the region of 450 nm. For effective degradation of RhB dye, 50 mg of catalyst was added the 100 mL (10 µM) of the RhB dye solution in a 150 mL reaction vessel. At given time intervals, 5 mL of aliquots was collected. The degraded solutions were analyzed using the absorption wavelength (λ_{\max}) at 553 nm. After the degradation, the catalyst was separated from the reaction mixture by filtering the reaction mixture and the catalyst was washed with ethanol and water for several times and dried to carry out the reusability tests.

Conclusions

Novel CuO/CS NCF were synthesized using solution cast method. The structure, morphology and optical properties were investigated in detail. Entrapping of CuO into the CS matrix amplified the band gap of the CuO. The photocatalytic activity and adsorption capacity of CuO/CS NCF were evaluated. The combinatorial effect of adsorption and photo degradation reflected in the enhanced photo reactivity which justified the importance of adsorption in photocatalysis. This excellent behaviour may be attributed to the large surface area of CuO/CS NCF and small crystalline size of CuO, which significantly facilitates diffusion and mass transportation of RhB molecules and delays the recombination time of photo-generated electron-hole pairs in the photocatalysis. The photocatalytic degradation system was not only restricted with RhB but also extended to CV and CR dyes. On the basis of results, the present system provides economically feasible and environmentally friendly method in the treatment of environmental pollutants.

Acknowledgements

The authors express their sincere thanks to the College managing board, Principal and Head of the Department, VHNSN College for providing necessary research facilities. The authors are also thankful to DST and saif IIT madras for providing ICP-OES facility.

Notes

^aDepartment of Chemistry, VHNSN College, Virudhunagar-626001, Tamil Nadu, India

^bRubber Technology Centre, Indian Institute of Technology, Kharagpur - 721302, India

^cSRM Research Institute, SRM University, Chennai-600025, Tamilnadu, India

^dIJN-UTM Cardiovascular Engineering Centre, Faculty of Bioscience and Medical Engineering, Universiti Teknologi Malaysia, Johor Bahru 81310, Malaysia

References

1. D. Ravelli, D. Dondi, M. Fagnonia, A. Albin, *Chem. Soc. Rev.*, 2009, **38**, 1999–2011.
2. S.G. Babu, R. Vinoth, B. Neppolian, D.D. Dionysiou, M. Ashokkumar, *J. Hazard. Mater.* 2015, **291**, 83–92
3. P.S. Kumar, M. Selvakumar, S.G. Babu, S. Karuthapandian, S. Chattopadhyay, *Mater. Lett.* 2015, **151** 45–48.
4. A. Fernandez, G. Lassaletta, V. M. Jimenez, A. Justo, A.R. Gonzalez-Elipe, J.M. Herrman, H. Tahiri, and Y. Aitlchou, *Appl. Catal. B: Environ.* 1995, **7**, 49-63.
5. C. Guillard, H. Lachheb, A. Houas, M. Ksibi, E. Elaloui, J.M. Herrmann, *J. Photochem. Photobiol. A: Chem.* 2003, **158**, 27-33.
6. H. Lachheb, E. Puzenat, A. Houas, M. Ksibi, E. Elaloui, C. Guillard, J.M. Herrmann, *Appl. Catal. B: Environ.* 2002, **39**, 75-90.
7. C. Guillard, J. Disdier, C. Monnet, J. Dussaud, S. Malato, J. Blanco, M.I. Maldonado, J. M. Herrmann, *Appl. Catal. B: Environ.* 2003, **46**, 319-332.
8. J.E. Hardy, S. Hubert, D.J. Macquarrie, A.J. Wilson, *Green Chem.* 2004, **6**, 53-56.
9. T. Vicent, E. Guibal, *Ind. Eng. Res. Chem.* 2002, **41**, 5158-5164.
10. J. Zhang, C.G. Xia, *J. Mol. Catal. A* 2003, **206**, 59-65.
11. M.Y. Yin, G.L. Yuan, Y.Q. Wu, M.Y. Huang, Y.Y. Jiang, *J. Mol. Catal. A* 1999, **147**, 93-98.
12. X.B. Zeng, Y.F. Zhang, Z.Q. Shen, *J. Polym. Sci. A* 1997, **35**, 2177-2182.
13. N.V. Kramareva, A.Y. Stakheev, O.P. Tkachenko, K.V. Klementiev, W. Grunert, E.D. Finashina, L.M. Kustov, *J. Mol. Catal. A* 2004, **209**, 97-106.
14. H. Zhu, R. Jiang, Y. Fu, Y. Guan, J. Yao, L. Xiao, G. Zeng, *Desalination* 2012, **286**, 41–48.
15. H. Zhua, R. Jianga, L. Xiao, Y. Chang, Y. Guan, X. Li, G. Zeng, *J. Hazard. Mater.* 2009, **169**, 933–940.
16. M. Selvakumar, S. K. Jaganathan, G. B. Nando, S. Chattopadhyay, *J. Biomed. Nanotechnol.* 2014, **10**, 1-15.
17. X. Liu, Z. Li, Q. Zhang, F. Li, T. Kong, *Mat. Lett.* 2012, **72**, 49–52.
18. J. Tang, Z. Zou, J. Ye, *Mater. Chem.* 2004, **16**, 1644-1649.
19. C.G.T. Neto, J.A. Giacometti, A.E. Job, F.C. Ferreira, J.L.C. Fonseca, M.R. Pereira, *Carbohydr. Polym.* 2005, **62**, 97–103.
20. D. Yang, J. Li, Z.Y. Jiang, L.Y. Lu, X. Chen, *Chem. Eng. Sci.* 2009, **64**, 3130–3137.
21. J.Y. Chen, P.J. Zhou, J.L. Li, Y. Wang, *Carbohydr. Polym.* 2008, **72**, 128-132.
22. C.Karunakaran, S.Karuthapandian, *Sol. Energy Mater. Sol. Cells* 2006, **90**, 1723-28
23. C.Karunakaran, S.Senthilvelan, S.Karuthapandian, *Sol. Energy Mater. Sol. Cells* 2005, **89**, 391-402

24. P. S. Kumar, M. Selvakumar, P. Bhagabati, B. Bharathi, S. Karuthapandian, S. Balakumar, *RSC Advances*, 2014, **4**, 32977–32986.